Dist: A

REPORT DOCUMENTATION PAGE

Form Approved
OMB No. 0704-0188

1. AGENCY USE ONLY (Leave blank)	2. REPORT DATE	3. REPORT TYPE AND DATES COVERED
	12/27/94	Final 11/1/91 - 10/31/94

4. TITLE AND SUBTITLE

Studies of Energy Transfer Processes of Relevance to Chemically and Optically Pumped Lasers

5. FUNDING NUMBERS

61102F 2303 ES

6. AUTHOR(S)

Michael C. Heaven

7. PERFORMING ORGANIZATION NAME(S) AND ADDRESS(ES)

Emory University
303B School of Dentistry
Atlanta, GA 30322

8. PERFORMING ORGANIZATION REPORT NUMBER

AFOSR-TR- 95 0017

9. SPONSORING/MONITORING AGENCY NAME(S) AND ADDRESS(ES)

AFOSR/~~NC~~ NL
Building 410, Bolling AFB DC
20332-6448
Dr Berman

10. SPONSORING/MONITORING AGENCY REPORT NUMBER

F49620-92-J-0073

11. SUPPLEMENTARY NOTES

12a. DISTRIBUTION/AVAILABILITY STATEMENT

APPROVED FOR PUBLIC RELEASE; DISTRIBUTION IS UNLIMITED.

12b. DISTRIBUTION CODE

A

13. ABSTRACT *(Maximum 200 words)*

The relaxation dynamics of vibrationally excited levels of $I_2(X)$ are of relevance to the chemical oxygen iodine laser (COIL). Rotational and vibrational energy transfer rate constants have been measured for selected levels with v">20. The collision partners He, Ar, I_2,Cl_2, O_2, and H_2O were investigated. A numerical model that relates state-to-state energy transfer rate constants to $I_2^{\dagger}$ deactivation processes in COIL has been developed. The results for H_2O show that the true deactivation rate constant is about an order of magnitude smaller than the estimate used in current computer simulations of COIL systems.

Energy transfer from $O_2(a^1\Delta)$ and $I(^2P_{1/2})$ to $I_2(X)$ has been investigated. The nascent vibrational distribution resulting from $I(^2P_{1/2})+I_2(X)$ collisions was characterized, and improved spectroscopic constants for the D state of I_2 are reported.

Jet-cooling and emission spectroscopy techniques have been used to characterize the D'(2)-A'(2) and β(1)-A(1) ion-pair to valence state transitions of iodine monobromide.

14. SUBJECT TERMS

Energy Transfer
Chemical Oxygen Iodine Laser

15. NUMBER OF PAGES

16. PRICE CODE

17. SECURITY CLASSIFICATION OF REPORT	18. SECURITY CLASSIFICATION OF THIS PAGE	19. SECURITY CLASSIFICATION OF ABSTRACT	20. LIMITATION OF ABSTRACT
UNCLASSIFIED	UNCLASSIFIED	UNCLASSIFIED	UNLIMITED

CONTENTS

Introduction

The Chemical Oxygen Iodine Laser (COIL) is the only demonstrated example of a chemically pumped electronic transition laser[1]. COIL systems, operating at a wavelength of 1.315 μm, provide very high energy laser beams. These devices normally function in a continuous mode, but can also be modulated rapidly by Zeeman gain-switching[2-4]. Recently, frequency doubling of a COIL device has been achieved[5]. Several military and commercial applications for COIL systems are being considered. Experimental programs aimed at increasing the efficiency of the oxygen-iodine laser and raising the working pressure of the device are currently in progress. In parallel with these efforts, computational models are being developed so that energy loss mechanisms may be identified, and methods for eliminating or reducing these problems may be explored[6]. Any realistic model of the laser can be divided into physical and chemical components. The physical part of the problem deals with reagent mixing and transport properties, while the chemical component deals with reactions that generate, excite, and deactivate atomic iodine[6-16]. At present, the reliability of computer modeling is compromised by unresolved questions regarding the I_2 dissociation mechanism, and the lack of rate constant data for several key processes.

In COIL systems, I_2 is dissociated by multiple collisions with electronically metastable species. It is thought that the two most important metastables in this process are $O_2(a^1\Delta)$ and $I(^2P_{1/2})$. However, the mechanism by which I_2 is dissociated in $I_2/O_2(a^1\Delta)$ mixtures has been the subject of several investigations, and of some controversy[7-15]. Despite these efforts, the mechanism is still not fully understood. As $O_2(a^1\Delta)$ does not posses sufficient energy to dissociate I_2 in a single collision, sequences involving energy pooling and multiple energy transfer events have been considered. Current theories[7-15] suggest that the first step may be the electronic to vibrational transfer (E-V) process

$$I_2(X) + O_2(a^1\Delta) \rightarrow I_2(X)\ v''\approx 33\text{-}44 + O_2(X) \qquad (1)$$

Subsequent collisions of $O_2(a^1\Delta)$ with $I_2(X)$ $v''>20$ can result in either direct dissociation, or electronic excitation of I_2 to the $A'(2_u)$, $A(1_u)$, or $B(0_u^+)$ states. There are then several reactions, generalized by the equations

$$O_2(a^1\Delta) + I_2^{\dagger} \rightarrow 2I + O_2(X) \qquad (2a)$$

$$O_2(a^1\Delta) + I_2^{*} \rightarrow 2I + O_2(X) \qquad (2b)$$

that can contribute to the dissociation. In these equations $I_2^{\dagger}$ denotes $I_2(X)$ $v''>20$, and I_2^{*} is electronically excited I_2. Once atomic I has been liberated, it is rapidly excited by the process

$$O_2(a^1\Delta) + I(^2P_{3/2}) \rightarrow I(^2P_{1/2}) + O_2(X) \quad (3)$$

In addition to being the species responsible for lasing, there are indications that $I(^2P_{1/2})$ also participates in the dissociation via the reactions

$$I(^2P_{1/2}) + I_2 \rightarrow I_2^{\dagger} + I(^2P_{3/2}) \quad (4)$$

and, possibly $$I(^2P_{1/2}) + I_2^{\dagger} \rightarrow 3I \quad (5)$$

The most extensive investigation of the dissociation mechanism was conducted by Heidner et al.[7], who used chemiluminescence to follow the concentrations of $I(^2P_{1/2})$, $I_2(A)$, $I_2(B)$, $O_2(a^1\Delta)$, and $O_2(b^1\Sigma^+)$ in a discharge flow-tube. This was the first study to show that slow "initiation" reactions preceded rapid I_2 dissociation, and that an unidentified excited state of I_2 was involved in the dissociation. Two distinct kinetic models were developed and evaluated by Heidner et al.[7] These differed considerably in the rate constants they assumed for generation and removal of excited I_2. Neither model gave an entirely satisfactory fit to the experimental data. Heidner et al.[7] considered the possibilities of the unidentified excited species being either $I_2(A')$ or $I_2^{\dagger}$. Problems were noted for either assignment. The kinetics indicated that the excited species was fairly stable, and almost immune to quenching by Ar. On the basis of physical intuition regarding vibrational relaxation, Heidner et al.[7] felt that the stability of the excited species was more consistent with $I_2(A')$. They were uncertain of this assignment, however, because the A' state lies too far above thermally populated $I_2(X)$ levels ($T_e(A')$=10042 cm^{-1}) to be excited by a single collision with $O_2(a^1\Delta)$.

The stability of $I_2^{\dagger}$ was probed in subsequent experiments. Hall et al.[10] reported a relatively large rate constant of 2.3×10^{-11} cm^3 s^{-1} for deactivation of $I_2(X, v''=40)$ by Ar. This result was not necessarily considered to be in conflict with the observations of Heidner et al.[7] Reactions 1 and 4 populate vibrational levels around v"=40, whereas transfer from $O_2(a^1\Delta)$ or $I(^2P_{1/2})$ can dissociate $I_2^{\dagger}$ from levels above v"=20. Therefore, many collisions may be needed to relax the nascent $I_2^{\dagger}$ to levels below v"=20. Indeed, David et al.[9] have shown that the flow-tube kinetics can be modeled using the rate constants of Hall et al.[10] Constraints required by the model were that relaxation proceeds via sequential v→v-1 steps, and that the rate constants for these steps scale linearly with v.

The models proposed by Heidner et al.[7] were intended to stimulate further research. They did not fully reproduce the experimental data, and were not unique. Even so, these models have provided estimates for several rate constants that have not been examined by other means. Consequently, computer models of COIL systems that have been developed at the Air Force Phillips laboratory, and by other research groups[6], have relied heavily on

the flow-tube rate constants. No doubt, some the shortcomings of the laser models can be traced to inaccuracies in the rate constant data base. Research carried out under grant AFOSR 49620-92-J-0073 was primarily directed towards the measurement of energy transfer processes of relevance to COIL systems

1. Spectroscopy and Electronic Energy Transfer Dynamics of I_2.

A. Spectroscopic studies of the I_2 D-X transition.

To perform energy transfer measurements on $I_2(X)$ v">20 we needed a sensitive, state-specific method for observing these highly excited vibrational levels. Laser induced fluorescence (LIF) of the intense D-X transition of I_2 proved to be ideal for this purpose, but it quickly became apparent that extension of the spectroscopic data base was an essential prerequisite for energy transfer studies. Problems traceable to the spectroscopic constants were encountered by Nota et al.[13] when they tried to extract population distributions from D←X spectra recorded in $O_2(a^1\Delta)/I_2$ mixtures. The available constants were not accurate enough for direct inversion of the line intensity data. Due to large differences between the X and D state equilibrium internuclear distances, transitions suitable for observing $I_2(X)$ levels in the range $20 \le v" \le 50$ terminate on the $0 \le v" \le 40$ vibrational levels of $I_2(D)$. Prior to the present studies, the most accurate data for the lower levels of $I_2(D)$ had been obtained from optical-optical double resonance (OODR) measurements[17]. The bands of interest for probing $I_2^\dagger$ were not well-characterized by this approach.

Two techniques were used to examine the $I_2(D)$ $(4 \le v' \le 37) \leftarrow X(23 \le v" \le 42)$ bands. In one series of experiments, photofragmentation of I_2Ar_n clusters was used to populate excited vibrational levels of the ground state[18] ($I_2^\dagger$ was ejected from the fragmenting clusters, see below). Very low rotational temperatures were attained, yielding relatively uncongested spectra. In the second series of experiments, two pulsed lasers populated a specific ro-vibrational level (v_i J_i) of $I_2(X)$ by stimulated emission pumping (SEP). A third laser was then used to observe D-X lines originating from v_i J_i, and nearby levels that were populated by collisions. This experimental configuration (shown in Figure 1) was developed for studies of inelastic collisions, but it also provided a convenient method for completing the spectroscopic ground-work. In all of the measurements, D-X spectra were excited by the frequency doubled output from a tunable dye laser. Absolute wavenumber calibration was achieved by using the fundamental of the dye laser to simultaneously record

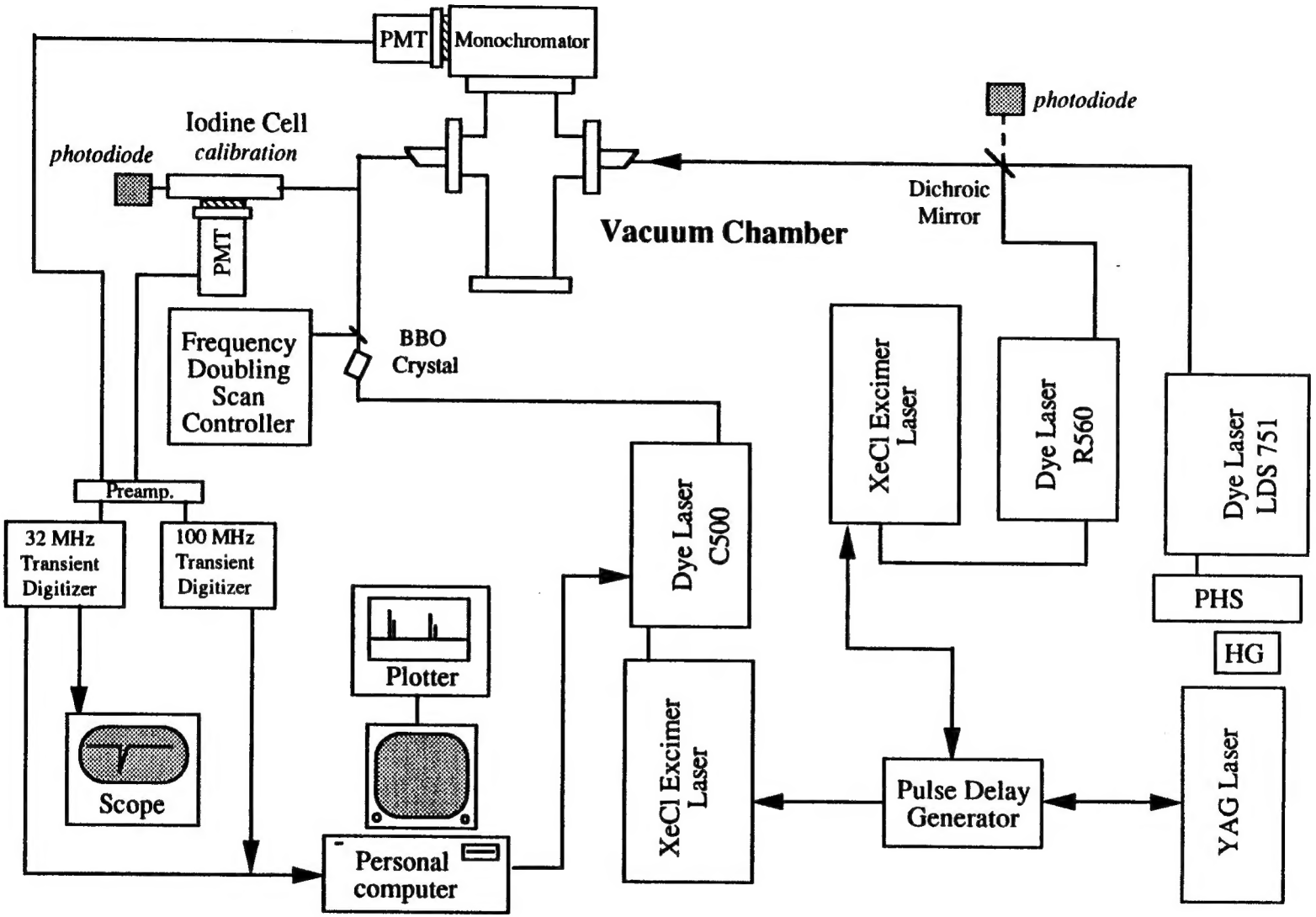

Figure 1. Experimental apparatus for studies of I_2 spectroscopy and energy transfer

the I_2 B-X spectrum. The positions of the B-X lines were taken from the work of Gerstenkorn and Luc[19].

Rotationally resolved spectra were recorded for the D-X bands $12 \geq v' \geq 5 \leftarrow v''=38$ and $37 \geq v' \geq 30 \leftarrow v''=23$. Band origins and rotational constants were obtained by fitting the line positions to the expression

$$\nu = \nu_{v',v''} + B_v' J'(J'+1) - B_v'' J''(J''+1) \qquad (1)$$

(trial fits to an expression that included the centrifugal distortion constants did not yield statistically significant values for these parameters). The lower state rotational constants were found to be in good agreement with those obtained by Bacis et al.[20] and Tellinghuisen et al.[21] As these earlier studies of the ground state were of greater accuracy than our measurements, the final fits to equation (1) were made with the lower rotational constants fixed at the values given by Bacis et al.[20] This scheme yielded D state rotational constants that were in excellent agreement with the values reported by Ishiwata and Tanaka[17]. Vibrational term energies for the D state were calculated by adding the ground state vibrational energies[20] to the fitted band origins. The resulting vibronic term energies (relative to the ground state minimum) are listed in Table 1. The new term energies were compared with energies predicted using the constants of Ishiwata and Tanaka[17]. At $v''=34$ the predicted energies were in error by 0.36 cm^{-1}. This error increased with decreasing v", reaching a value of 1.77 cm^{-1} at $v'=5$. Comparisons with energies predicted from the constants of Bartels et al.[22], and Hoy and Lipson[23] revealed essentially the same discrepancies. To put this in perspective, a predictive accuracy of ± 0.08 cm^{-1} is needed for the inversion of line intensity data from congested spectra.

To obtain improved spectroscopic constants for $I_2(D)$, we combined our results with the best available data for the levels above $v'=37$. Ishiwata and Tanaka[17] noted that their data were most accurate for the range $76 \leq v' \leq 124$. For these levels they reported that the standard deviation of a global fit was 0.052 cm^{-1}. Vibronic term energies for the ranges $125 \leq v' \leq 201$ and $202 \leq v' \leq 290$ were taken from the studies of Bartels et al.[22] and Hoy and Lipson[23], respectively. The complete set of vibronic term energies were fit to the standard Dunham expression

$$T^D(v) = \sum_n Y_{n,0}(v+1/2)^n$$

The data were weighted according to the inverse squares of their standard deviations $(1/(0.15\ cm^{-1})^2$ for $v' \leq 124$; $1/(0.5 cm^{-1})^2$ for $v' \geq 125)$. A satisfactory fit was achieved using a ninth order polynomial. As the constants obtained were highly correlated, they

Table 1

Vibrational Term Energies for $I_2(D)$

v'	$\nu(cm^{-1})$	$\delta(cm^{-1})^a$
4	41451.97	0.15
5	41545.84	0.13
6	41639.56	0.13
7	41733.01	0.14
8	41826.28	0.08
9	41919.19	0.13
10	42011.95	0.15
11	42104.47	0.14
30	43810.37	0.15
31	43897.37	0.14
32	43984.05	0.11
33	44070.47	0.09
34	44156.55	0.09
35	44242.35	0.11
36	44327.85	0.14
37	44413.09	0.13

a. 1-σ errors from fits to equation 1.

were subjected to a systematic rounding procedure that preserves their accuracy[24]. The final constants are given in Table 2, where they are compared with several previous estimates. The residuals of the fit, determined for the rounded constants, are plotted in Figure 2. The 1-σ statistical error band for the fitted $T^D(v)$ function is shown in Figure 3. Differences between the D state energies calculated from the present results, and those from the constants of Ishiwata and Tanaka[17] ($\delta T^D(v)=T^D(v)_{present}-T^D(v)_{ref.\ 17}$) are also plotted in Figure 3. Local fitting problems are primarily responsible for the deviations. The previous constants work well over the ranges of levels from which they were defined. For the purpose of extracting vibrational populations from D-X band intensity data, we have calculated a new RKR curve for the D state, and a matrix of the relevant D-X Franck-Condon factors. These results are listed in the appendix of this report.

B. Spectroscopy and relaxation of I_2Ar_n clusters. Geminate recombination and cluster fragmentation.

I_2Ar_n clusters were studied in a free-jet expansion. When excited to states that correlated with the first ion-pair manifold of I_2, the clusters yielded visible and near UV emissions. The ion-pair states were accessed by 193 nm excitation of ground state clusters, or near UV excitation of electronically metastable $I_2(A' \text{ or } A)Ar_m$. Comparisons of the cluster and I_2/Ar matrix spectra suggested that such excitations result in fragmentation and "melting" of the clusters prior to emission.

532 nm photodissociation of I_2 within the clusters was followed by geminate recombination that populated the A', A, and X states. The probability for ejection of the recombined I_2 from the clusters during the relaxation process appeared to be size dependent. These results represent tentative steps towards the study of $I(^2P_{3/2}) + I(^2P_{3/2})$ recombination in Ar clusters. They also indicate that dissociation, recombination, fragmentation processes may be used as a general method for generating metastable species in supersonic expansions. This work is described in reference 18.

C. Energy transfer from $I(^2P_{1/2})$ to $I_2(X)$

Pulsed photolysis and laser probing techniques were used to study the nascent state distribution resulting from $I_2(X) + I(^2P_{1/2}) \rightarrow I_2^\dagger + I(^2P_{3/2})$. Similar experiments had been conducted by Hall et al.[10], but the spectra obtained were not rotationally resolved. In our recent work, $I(^2P_{1/2})$ atoms were generated by using 490 nm light to photodissociate I_2 via the B state continuum. After a short delay (typically 1μs for a 100 mTorr sample), $I_2^\dagger$

Table 2
Electronic Term Energies and Vibrational Constants for $I_2(D)$ (cm^{-1})

Constant	Present work	Ref. (31)	Ref. (17)	Ref. (22)	Ref. (23)
$Y_{00}(T_e)$	41026.49(7)	41026.4(4)	41028.584(47)	41028.584(47)	41028.542(72)
$Y_{01}(\omega_e)$	95.0425(155)	95.66(21)	94.9928(60)	95.0108(286)	94.99697(1149)
$Y_{02}(-\omega_e x_e)$	-0.1057(10)	-0.1345(50)	-0.10919(26)	-0.11008(155)	-0.108789(590)
$Y_{03}/10^{-4}$	-7.832(276)	-2.14(43)	-5.805(50)	-5.759(310)	-6.1458(1378)
$Y_{04}/10^{-6}$	7.942(450)	1.3(2)	3.686(43)	3.936(287)	4.4999(1706)
$Y_{05}/10^{-9}$	-52.72(438)	-1.7(2)	-7.61(13)[b]	-11.22(124)	-15.718(1194)
$Y_{06}/10^{-11}$	26.0(26)	-	-	1.367(204)	3.289(474)
$Y_{07}/10^{-14}$	-83.5(91)	-	-	-	-3.64(10)
$Y_{08}/10^{-16}$	15.1(17)	-	-	-	0.130(86)
$Y_{09}/10^{-18}$	-1.16(14)	-	-	-	-

a. The 1σ uncertainties for these constants are given in parentheses
b. Due to a typographical error this is given as a positive constant in reference 17.

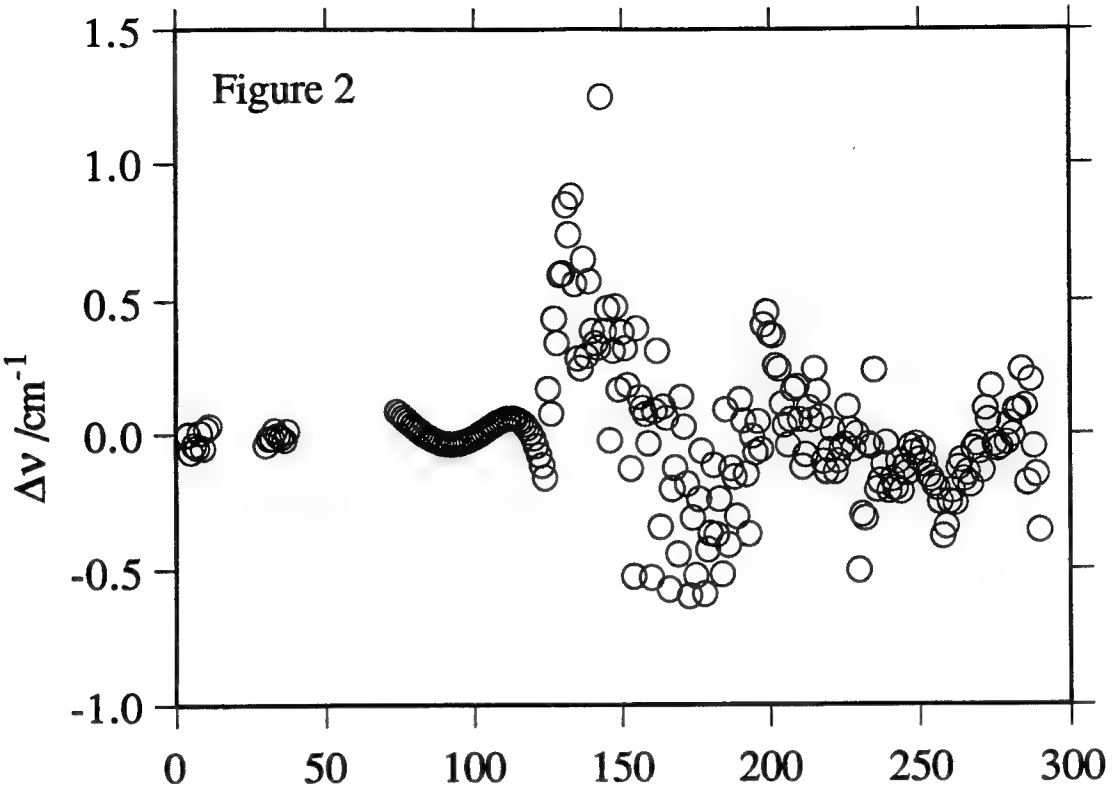
Figure 2
1.5
1.0
0.5
0.0
-0.5
-1.0
Δν /cm-1
0
50
100
150
200
250
300

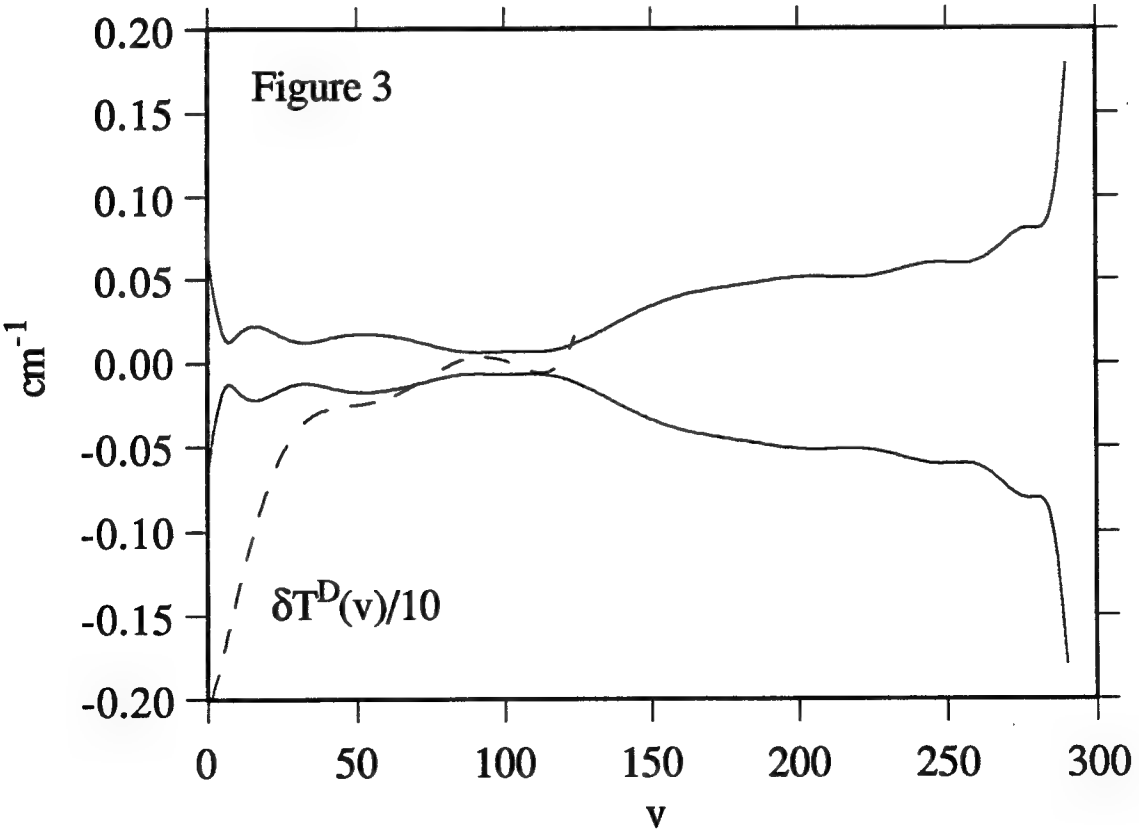
Figure 3
0.20
0.15
0.10
0.05
0.00
-0.05
-0.10
-0.15
-0.20
cm-1
δTD(ν)/10
0
50
100
150
200
250
300
ν

levels populated by E-V transfer were probed by recording rotationally resolved D-X spectra.

The new molecular constants for the D state were used to determine the product state distribution from an inversion of the line intensity data. Within each vibrational level the rotational populations were well represented by a Boltzman distribution with a temperature of 310±20 K. The nascent vibrational state population distribution is shown in Figure 4. Note that the distribution peaks at v"=40, which coincides with near resonant energy transfer, and cuts-off abruptly above v"=47. The distribution obtained from these measurements has been used in the determination of $I_2^\dagger$ deactivation rate constants from state-to-state transfer rate constants (see below).

D. Energy transfer from electronically excited oxygen to $I_2(X)$

An attempt to examine $I_2(X) + O_2(a^1\Delta) \rightarrow I_2^\dagger + O_2(X)$ E-V energy transfer was made. For this purpose, $O_2(a^1\Delta)$ was generated by using 248 nm pulses from a KrF laser to photodissociate O_3 in flowing O_3/I_2 mixtures. As in the experiments described above, a tunable probe laser was used to examine the I_2^* product state distribution by exciting the valence to ion-pair transitions. Unexpectedly, the probe laser spectra were dominated by the I_2 D'-A' bands. Observation of these bands depended on the photolysis of O_3, and it was verified that the A' state was not being populated by an indirect mechanism involving 248 nm excitation of I_2. The rate at which the A' state was excited was consistent with a single collision event. High yields of $O(^1D)$ atom are produced by photolysis of O_3 at 248 nm. The transfer process $O(^1D)+I_2(X) \rightarrow I_2(A')+O(^3P)$ could account for the appearance of $I_2(A')$, but it is unlikely that this channel is significant. It is known that O atoms react rapidly with I_2 to form IO+I. If a parallel energy transfer channel does exist, it is more likely to proceed by the near-resonant $O(^1D)+ I_2(X) \rightarrow I_2(B)+O(^3P)$ path. An alternative A' state excitation mechanism becomes apparent when the excess energy delivered by the photolysis pulse is considered. The energetic threshold for dissociation of O_3 into $O(^1D)+O_2(a^1\Delta)$ is 32,260 cm^{-1}, so 248 nm light provides about 8062 cm^{-1} of excess energy. When this is partitioned between the recoiling fragments, the $O_2(a^1\Delta)$ fragment will receive about 2700 cm^{-1}. Combined with the electronic energy, this sufficient to open the channel $O_2(a^1\Delta)^*+I_2(X) \rightarrow I_2(A')+O_2(X)$.

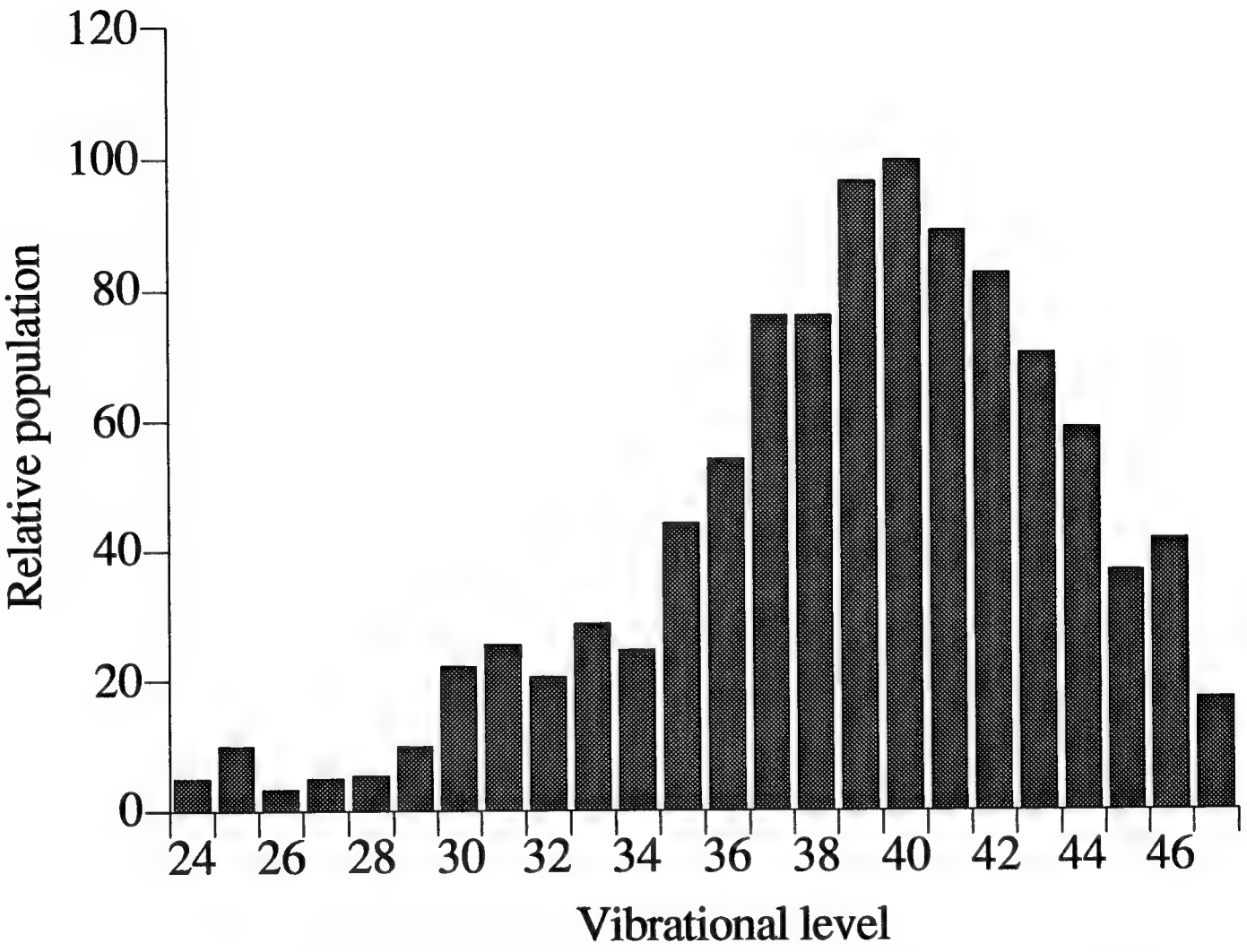

Figure 4. Vibrational population distribution resulting from $I_2(X)+I(^2P_{1/2})$ collisions.

2. Rotational and Vibrational Relaxation of $I_2^\dagger$

A. Experiment and results

Conceptually, the technique used to study inelastic collisions involving $I_2^\dagger$ was straightforward[25]. Figure 1 shows one variant of the apparatus used. Pulsed lasers were used to excite a single ro-vibrational level of $I_2(X)$ by stimulated emission pumping (SEP). After a suitable delay, molecules in the initially excited level, and in levels populated by collisions, were detected by a third laser that excited the D-X transition. A small monochromator (0.25 m) was used to selectively detect the D-X fluorescence.

In order to study rotational and vibrational energy transfer, a small amount of I_2 (typically 10-25 mTorr) was mixed with 0.05-1 Torr of a collision partner. Probe laser spectra were then recorded for a number of fixed delays between the state preparation and probe laser pulses. The energy transfer processes examined involved I_2 in one of the initial levels (v"=23, J"=57), (v"=38, J"=57), or (v"=42, J"=17), colliding with He, Ar, I_2, O_2, N_2, Cl_2 or H_2O. Self transfer was examined using an I_2 pressure of 200 mTorr. Figure 5 shows a typical probe laser spectrum. This trace was recorded for a mixture of 20 mTorr of I_2 with 60 mTorr of H_2O. The delay between the dump pulse and probe pulses was 200 ns. Lines originating from levels populated by rotational energy transfer are prominent in this trace. Weaker features produced by v"=23→22 relaxation can also be seen (note that vibrational transfer occurred with very little change in the angular momentum).

For each combination of an initial level and a collision partner, the total removal rate constant was determined by fixing the probe laser to monitor the initial level, and monitoring the fluorescence intensity as a function of dump-probe pulse delay time. Good single exponential decays were observed. Decay rates were determined by fitting to the expression $I(t) = Ae^{-kt}$, where A is a constant and $k = k_{I_2}'[I_2] + k'_M[M]$. k_{I_2}' and k'_M are the total transfer rate constants for collisions with I_2 and M, respectively. Rate constants, derived from Stern-Volmer plots, are listed in Table 3. All $M \neq I_2$ rate constants were corrected for self-transfer.

Rate constants for state-to-state ro-vibrational energy transfer ($v_i\ J_i \rightarrow v_f\ J_f$) were determined from rotationally resolved spectra taken under single collision conditions. An indirect method was used to verify that multiple collision events were not modifying the intensity distributions seen in these experiments. Spectra were taken at a variety of pressures and delay times for each collision partner, and conditions where the intensities of the collisionally populated spectral features began to show non-linear time or pressure

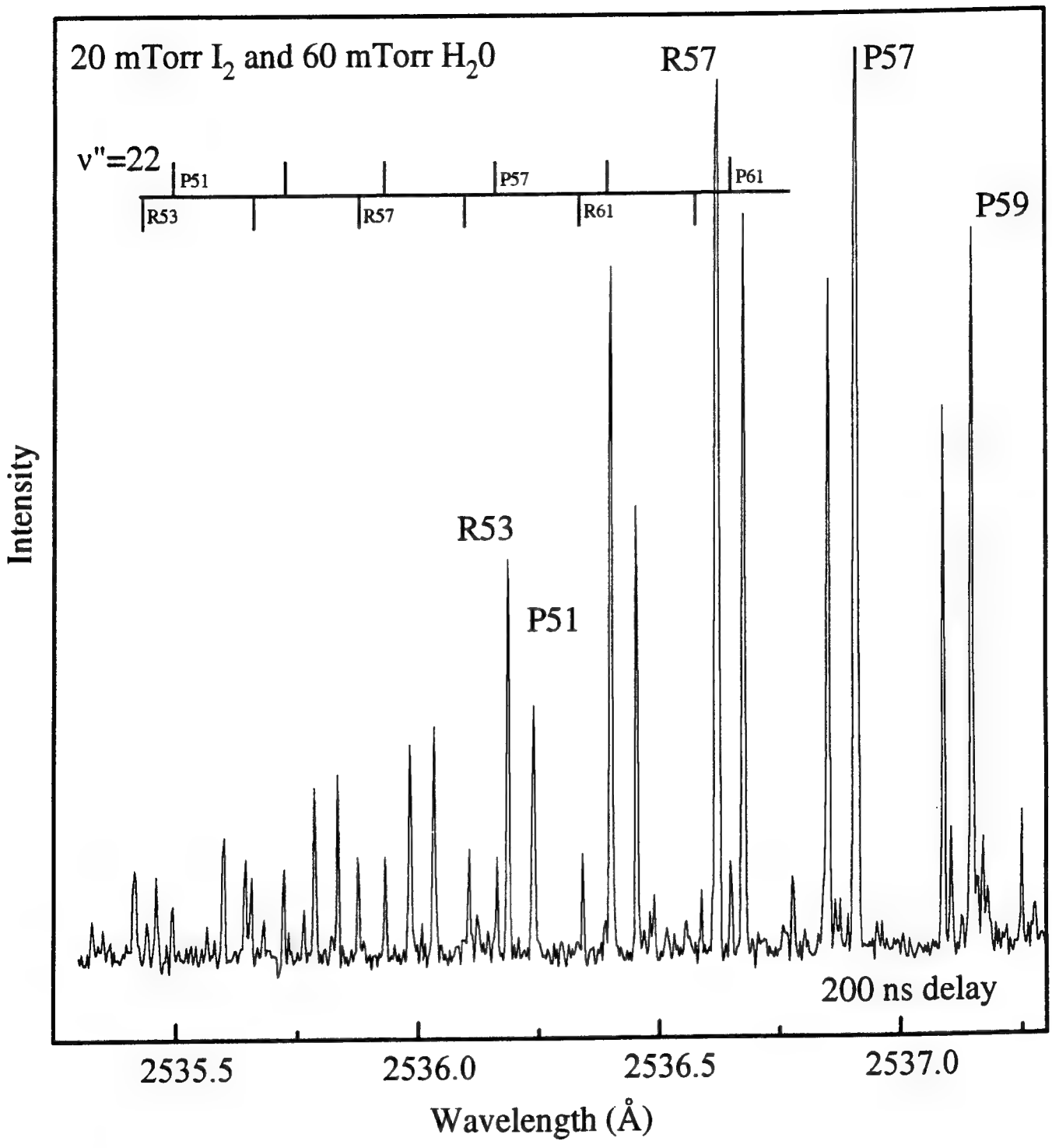

Figure 5. I_2 D-X spectrum showing levels populated by rotational and vibrational energy transfer

Table 3

Rate Constants for Population Loss from Individual Ro-Vibrational Levels of $I_2(X)$

Collision partner	$k_T(v=23, J=57)^a$	$k_T(v=38, J=49)^a$	$k_T(v=42, J=17)^a$
He	6.4	5.4	6.6
Ar	5.7	5.5	5.0
I_2	8.7	6.6	8.6
O_2	7.1	7.0	7.8
Cl_2	-	4.0	-
N_2	6.7	8.0	-
H_2O	9.3	8.8	-

a. Rate constants in units of 10^{-10} cm^3 s^{-1}. The estimated uncertainties are $\pm 0.5 \times 10^{-10}$ cm^3 s^{-1}.

dependence were identified. Spectra used to characterize energy transfer were then recorded at pressure-delay combinations that were well below those that revealed the effects of multiple collisions.

B. Data analysis

Computer simulations of the pump-dump-probe spectra were used to estimate the state-to-state energy transfer rate constants. The computer model was based on a kinetic analysis that assumed single collision conditions and that collisions with a single species, M, dominated. Starting with all of the molecules in the prepared level $v_i\ J_i$, the equations that describe the time evolution of the ground state population distribution are

$$\frac{-d[v_i\ J_i]}{dt} = k_i[v_i\ J_i], \qquad \text{and} \qquad \frac{d[v_f\ J_f]}{dt} = k_f[v_i\ J_i]$$

where $[v_i\ J_i]$ and $[v_f\ J_f]$ are the populations in the initial and final states, respectively. Constants k_i and k_f are defined by the equations

$$k_i = \sum_{v_f} \sum_{J_f} k_M(v_i\ J_i \rightarrow v_f\ J_f)[M] \qquad \text{and} \qquad k_f = k_M(v_i\ J_i \rightarrow v_f\ J_f)[M]$$

where $k_M(v_i\ J_i \rightarrow v_f\ J_f)$ is a state-to-state transfer rate constant. Integration of the rate equations yields the results

$$[v_i\ J_i] = [v_i\ J_i]_0\ e^{-k_i t} \qquad \text{and} \qquad [v_f\ J_f] = [v_i\ J_i]_0 \frac{k_f}{k_i}(1 - e^{-k_i t})$$

Ro-vibrational population distributions, calculated from the above equations and trial values for the rate constants, were used to generate synthetic spectra that could be compared with the experimental results. In principle, all of the rate constants could be varied until an optimum fit was achieved. However, the quality of our data was not sufficient to warrant this approach. Consequently, we used scaling laws to parameterize the rate constants, and then adjusted the parameter values to obtain agreement with experiment. For analysis of the pure rotational transfer data, a simplified version of the statistical power gap law[26] (SPG) was used, vis

$$k_M(J_i \rightarrow J_f) = C\ N_\Delta\ |\Delta E/B|^{-\gamma}$$

(in this equation the v_i=v_f labels have been omitted). C and γ are fitted parameters. B is the rotational constant, ΔE is the difference in energy between the initial and final states, and N_Δ is a statistical factor that depends on the extent to which the angular momentum projection quantum number, m, is modified by collisions. On the basis of on this

relationship, graphical simulations were used to obtain best estimates for the parameters C and γ. The C coefficients were constrained to give total rotational transfer rate constants ($k_{rot} = \sum_{J_f} k_M(J_i \rightarrow J_f)$) that were compatible with the decay rate constants given in Table 3. One set of fittings was performed with the assumption that m is randomized by collision. A second set was made with the constraint that $\Delta m=0$. We found that transfer induced by the atomic collision partners was consistent with $\Delta m=0$. For the molecular collision partners, fits obtained with the assumption of m-randomizing events were slightly better than those obtained with $\Delta m=0$. Rotational energy transfer parameters are collected in Table 4.

Vibrational energy transfer was typically an order of magnitude slower than rotational energy transfer. In the studies conducted to date, we have only observed $\Delta v=-1$ events. Upward transfer or multi-quantum downward transfer was not detected. Rotational contours of the bands originating from the $\Delta v=-1$ levels reflected a tendency to conserve angular momentum. From trial simulations it was found that rate constants defined by the expression

$$k_M(v_i\ J_i \rightarrow v_i\text{-}1\ J_f) = C_{v \rightarrow v\text{-}1}\ N_\Delta\ |\Delta E_{rot}/B|^{-\gamma}$$

yielded distributions that were in good agreement with experiment. Here, ΔE_{rot} is the difference in rotational energy between the initial and final states. Note that the equation has a singularity at $\Delta E_{rot}=0$. This problem was avoided by setting $k_M(v_i\ J_i \rightarrow v_{i-1}\ J_i) = k_M(v_i\ J_i \rightarrow v_{i-1}\ J_i+2)$. The values of γ used in these simulations were taken from Table 4, leaving only the $C_{v \rightarrow v-1}$ coefficients to be determined from the fits. Overall rate constants for transfer from v_i to v_i-1 were evaluated by summing the state-to-state rate constants. Vibrational transfer rate constants are given in Table 5.

C. Modeling of $I_2^\dagger$ deactivation

After the slow initiation stage, the primary channel for excitation of $I_2^\dagger$ in COIL systems is $I_2(X) + I(^2P_{1/2}) \rightarrow I_2^\dagger + I(^2P_{3/2})$. We have shown that levels in the range of $25 \leq v'' \leq 46$ are populated by this process. The energy carried by $I(^2P_{1/2})$ or $O_2(^1\Delta)$ metastables is sufficient to dissociate I_2 from levels with $v'' \geq 20$. However, David et al.[9] have suggested that only levels $v''=30$ and higher are efficiently dissociated, due to Franck-Condon restrictions. In modeling the deactivation process, we have treated the level that defines the threshold for efficient dissociation (v_{th}) as a variable parameter. Hence, the rate at which $I_2^\dagger$ is deactivated corresponds to the rate at which the nascent distribution (c.f. Figure 4) is relaxed to levels below v_{th}.

Table 4

Rotational Energy Transfer Rate Constants and Statistical Power Gap Law Model Parameters for $I_2(X)$.

	v=23, J=57			v=38, J=49		
Collision partner	k_{rot}[a]	α	N_Δ[b]	k_{rot}[a]	α	N_Δ[b]
He	5.2	0.60	$2J_<+1$	4.4	0.54	$2J_<+1$
Ar	5.4	0.67	$2J_<+1$	5.1	0.65	$2J_<+1$
I_2	8.7	0.43	$2J_f+1$	6.0	0.71	$2J_f+1$
O_2	-	-	-	6.3	0.66	$2J_f+1$
Cl_2	-	-	-	3.1	0.76	$2J_f+1$
H_2O	-	-	-	6.2	0.94	$2J_f+1$

a. Rate constants for transfer to all other rotational levels of v_i. Constants are given in units of 10^{-10} cm^3 s^{-1}.

b. $J_<$ is the smaller value of J_i or J_f. This statistical factor is associated with m-conserving collisions

Table 5

Vibrational Energy Transfer Rate Constants ($\Delta\upsilon$=-1) for $I_2(X)$.

Collision partner	$k(\upsilon''=23)^a$	$k(\upsilon''=38)^a$
He	1.2	1.0
Ar	0.3	0.4
I_2	0.5	0.6
O_2	--	0.7
Cl_2	--	0.9
H_2O	1.7	2.6
D_2O	--	2.1

a. Rate constants in units of 10^{-10} cm^3 s^{-1}.

The relationship between the measured state-to-state vibrational energy transfer rate constants and the deactivation rate constant has been examined by computer modeling. The model was based on the following assumptions:

(i) Vibrational energy transfer is controlled by the v_f-v_i=±1 selection rule.

(ii) The rate constants for downward transfer ($k_{v\to v-1}$) are dependent on the vibrational quantum number in a simple manner, e.g. linear (Landau-Teller) scaling; $k_{v\to v-1} = vk_{1\to 0}$, or power law scaling; $k_{v\to v-1} = v^n k_{1\to 0}$.

(iii) Upward energy transfer rate constants can be calculated from detailed balance;

$$k_{v-1\to v} = k_{v\to v-1}\exp(-(E_v - E_{v-1})/k_bT).$$

(iv) The rotational distributions are thermalized and do not need to be considered.

The initial (time=0) distribution of population among the $I_2(X)$ vibrational levels was defined using the data from Figure 4. The number densities were arbitrarily chosen to give a total number density (summed over all vibrational levels) of $3x10^{10}$ cm^{-3} (the relaxation kinetics do not depend on the I_2 pressure in this model).

Coupled rate equations that describe the vibrational energy transfer processes are defined by

$$\frac{d[I_2,v]}{dt} = \left(k_{v-1\to v}[I_2,v-1] + k_{v+1\to v}[I_2,v+1] - \left(k_{v\to v+1} + k_{v\to v-1}\right)[I_2,v]\right)[M]$$

These equations were solved by numerical integration. At equally spaced time intervals the $I_2^\dagger$ number density was obtained from the summation $[I_2^\dagger] = \sum_{v=v_{th}}^{59}[I_2,v]$.

Figure 6 shows a typical $[I_2^\dagger]$ vs time profile for relaxation by He. This calculation was performed with linear v-scaling (n=1), $k_{0\leftarrow 1}$=$3.9x10^{-12}$ cm^3 s^{-1} (extrapolated from the SEP data), an He pressure of 5 Torr, and T=298 K. As expected, the $[I_2^\dagger]$ time dependence was a "sigmoid-like" function; $[I_2^\dagger]$ does not begin to decay noticeably until a significant fraction of the population has relaxed to levels near v=20. Characteristic lifetimes for these curves were defined by

$$\tau = \frac{\int_0^\infty [I_2^\dagger]_c\, t\, dt}{\int_0^\infty [I_2^\dagger]_c\, dt}$$

where $[I_2^\dagger]_c$=$[I_2^\dagger]$ - $[I_2^\dagger]_{t=\infty}$, and $[I_2^\dagger]_{t=\infty}$ is the thermal population of the $v\geq v_{th}$ levels at equilibrium. For the curve shown in Figure 6, this expression gives τ= 1.2 μs.

To begin with, the model was used to examine the possibility that the overall deactivation process could be represented using a single effective rate constant ($k_M^\dagger$) for

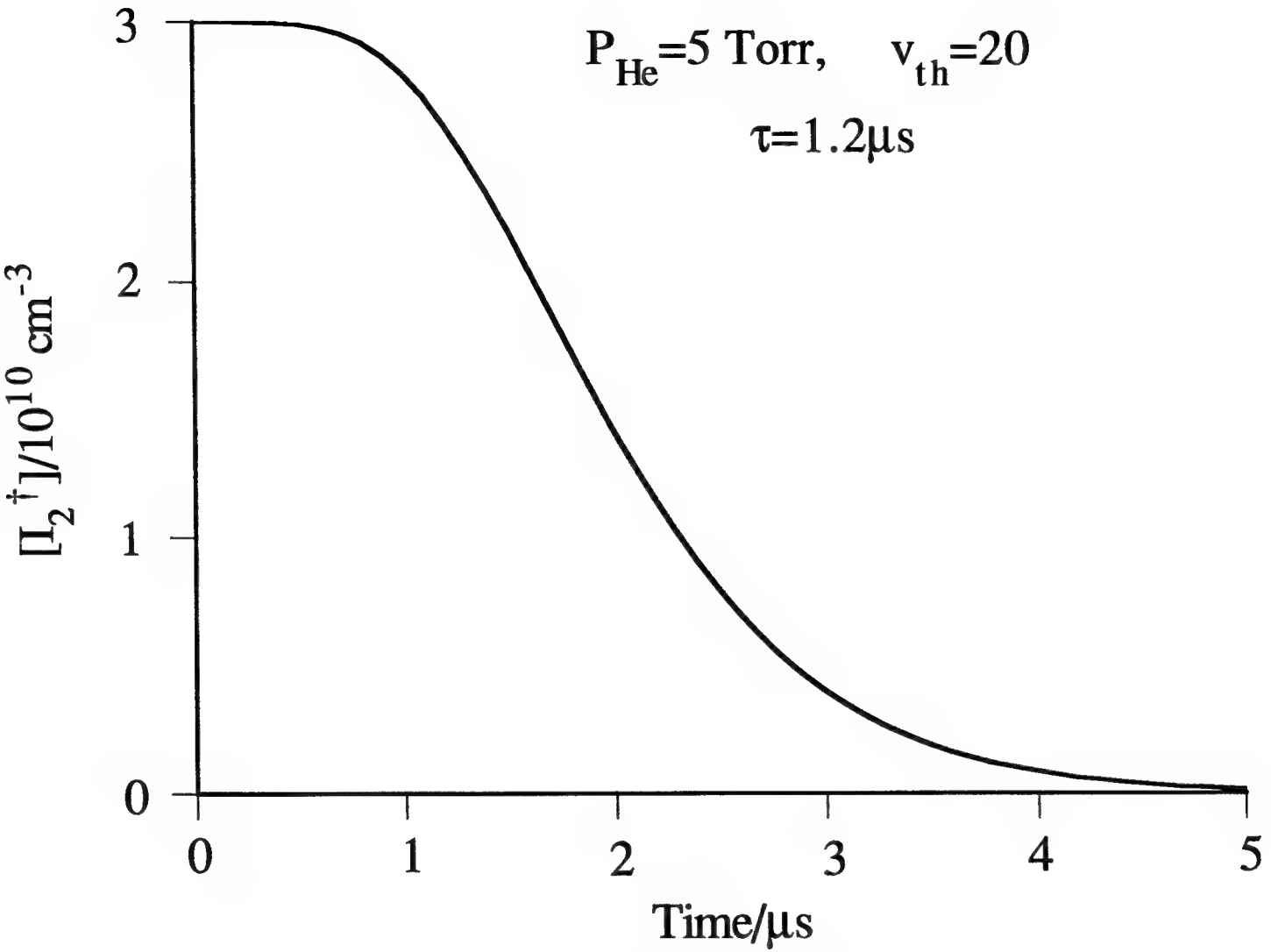

Figure 6. Typical $I_2^\dagger$ concentration profile from model calculations.

each collision partner. Plots of $1/\tau$ vs. collider-gas pressure were found to be linear, thereby demonstrating the validity of the concept of a deactivation rate constant.

Deactivation rate constants were calculated from the measured vibrational energy transfer rate constants for He, Ar, Cl_2, O_2, and H_2O. The results are collected in Table 6. Deactivation rate constants are given for the limiting cases of v_{th}=20 and v_{th}=30. The power scaling (n) used for each calculation was chosen in accordance with the available data. For He, the measurements suggest that the v→v-1 rate constants are almost independent of v over the range 20<v"<40. However, Table 6 lists both n=0 and n=1 results for He, in order to illustrate the effect on $k_M^\dagger$ of increasing n from 0 to 1. These calculations show that, provided the base rate constant ($k_{1\rightarrow 0}$) is consistent with the measured rate constants, changing n from 0 to 1 does not greatly influence the deactivation rate constants.

D. Significance of Deactivation Rate Constants for COIL Models.

Previous models of COIL systems have used a standard set of estimated rate constants (AFWL rate package)[16]. The present results require one significant change in this data base. The AFWL package uses a rate constant for deactivation of $I_2^\dagger$ by H_2O of $3x10^{-10}$ cm^3 s^{-1}. Based on the results given in Table 6, we recommend a value of $k_{H_2O}^\dagger$=$1.5x10^{-11}$ cm^3 s^{-1}.

The rate constant for deactivation by O_2 was estimated at $5x10^{-11}$ cm^3 s^{-1}, and the present results are consistent with this value.

As He is used as the carrier gas in most high-power COIL devices, the deactivation rate constant for He is a critical parameter. The AFWL rate package uses $k_{He}^\dagger$=$4x10^{-12}$ cm^3 s^{-1}, while the present results indicate a slightly higher value, within the range $0.5 \le k_{He}^\dagger \le 1.0x10^{-11}$ cm^3 s^{-1}. Carrol[16] and co-workers have suggested that $k_{He}^\dagger$ may be larger still. Beyond an optimal pressure, COIL output power decreases with increasing pressure. Carrol[16] examined the possibility that $I_2^\dagger$ deactivation by He was primarily responsible for this behavior. In order to duplicate the observed pressure dependence, Carrol[16] found that $k_{He}^\dagger$ needed to be increased to $4.8x10^{-11}$ cm^3 s^{-1}, when this was the only rate constant allowed to deviate from the AFWL values. These calculations were performed before data from the energy transfer measurements were available. Since the fitted value for $k_{He}^\dagger$ was not consistent with the present results, a model with two variable rate constants is being investigated. In the latest calculations, $k_{He}^\dagger$ and the rate constant (k_{25}) for $I_2^\dagger + O_2(a^1\Delta) \rightarrow I + I + O_2(^3\Sigma)$ are allowed to vary, and a corrected value for

Table 6

Effective Deactivation Rate Constants (298 K)

Collision partner	n	$k_{1\rightarrow 0}$[a]	$k^{\dagger}(v_{th}=20)$[b]	$k^{\dagger}(v_{th}=30)$[b]
He	0	12	5.4	8.3
He	1	0.39	5.1	9.8
Ar	1	0.12	1.6	2.9
O_2	0	7.0	3.3	4.9
Cl_2	0	9.0	4.1	6.3
H_2O	1	0.71	9.3	17

a. Units of 10^{-11} cm^3 s^{-1}.

b. Units of 10^{-12} cm^3 s^{-1}.

$k^{\dagger}_{H_2O}$ is used. Respectable fits to the pressure dependence have been achieved[27] using $k_{25}=1.8\times10^{-10}$ cm^3 s^{-1} and $k^{\dagger}_{He}=1.6\times10^{-11}$ cm^3 s^{-1}. The former is reduced from the AFWL value by a factor of 0.6. In the absence of experimental data for k_{25}, this adjustment seems reasonable. By reducing k_{25}, $k^{\dagger}_{He}$ is brought much closer to the energy transfer estimate. It is probable that even better agreement could be attained by treating more of the uncertain rate constants as variables.

Deactivation of $I_2^{\dagger}$ by Cl_2 was not considered in the AFWL package as it was thought that Cl_2 was completely consumed in the $O_2(a^1\Delta)$ generator. Recent experiments suggest that Cl_2 is not fully utilized when $O_2(a^1\Delta)$ generators are run at high pressures[28]. Furthermore, there was speculation that rapid deactivation of $I_2^{\dagger}$ by Cl_2 could be one of the factors that caused the loss of power seen at high pressures. The energy transfer measurements show that Cl_2 is not particularly effective in deactivating $I_2^{\dagger}$. If the presence of Cl_2 is causing a loss of laser power, it does not appear to operate by suppressing the dissociation of I_2.

3. Spectroscopy of Iodine Monobromide.

The A $1(^3\Pi)$ and A' $2(^3\Pi)$ states of IBr were observed in a free-jet expansion of IBr in Ar, following photolysis with ArF laser irradiation.

Laser excitation spectra were recorded for the $D'\,2(^3P_2) \leftarrow A'$ transition. The data included high-resolution, rotationally analyzed measurements for 34 bands of $^{127}I^{79}Br$ and 37 bands of $^{127}I^{81}Br$, plus bandhead measurements for >300 bands recorded in low-resolution. The data span $v'' = 0$-5 and $v' = 24$-97. Results from the analysis of these data were merged with preliminary results from a study of the $D' \rightarrow A'$ emission spectrum to yield spectroscopic constants valid for $v' = 0$-97, $v'' = 0$-22. The primary spectroscopic constants (cm^{-1}) were: $\Delta T_e = 28\,018.98$, $\omega_e' = 123.088$, $\omega_e x_e' = 0.2820$, $B_e' = 0.02853$, $\omega_e'' = 147.633$, $\omega_e x_e'' = 1.258$, $B_e'' = 0.04298$. This work is described in reference 29.

Excitation spectra were obtained for the $\beta\ 1(^3\Pi_2) \leftarrow$ A transition in medium (0.5 cm^{-1}) and high (0.08 cm^{-1}) resolution. Sixteen v'-v'' bands recorded in high resolution were rotationally analyzed, providing the first detailed characterization of the lowest three v levels in the A state. An additional 50 bandheads of the $v''=0$ and 1 progressions were recorded for both $I^{79}Br$ and $I^{81}Br$. The new data, which sample v' levels in the 31-71 range, were combined with existing information for low v in the β state to provide improved constants for the β state. These results were merged with least-squares

parameters from a reanalysis of existing data for the A and X states to yield spectroscopic parameters valid for υ=0-20 in the X state and υ=0-26 in the A state. Among these results are the first precise estimates of the equilibrium parameters for the A state: T_e=12369.68(14) cm^{-1}, ω_e=134.22(13) cm^{-1}, B_e=0.04240(5) cm^{-1}, R_e=2.8583 Å. This work is described in reference 30.

References.

1. See, for example, W. E. McDermott, N. R. Pchelkin, D. J. Benard, and R. R. Bousek, *Appl. Phys. Lett.* 32, 469 (1978); D. J. Benard, W. E. McDermott, N. R. Pchelkin, and R. R. Bousek, *Appl. Phys. Lett.* 34, 40 (1979); R. J. Richardson and C. E. Wiswall, *Appl. Phys. Lett.* 33, 138 (1979); J. Bacher and S. Rosenwaks, *Appl. Phys. Lett.* 41, 16 (1982)

2. G. D. Hager, D. Kopf, B. S. Hunt, B. Anderson, C. Woolhiser, and P. Crowell, *IEEE J. Quant. Elec.* 29, 933 (1993)

3. G. D. Hager, D. Kopf, B. S. Hunt, B. Anderson, and P. Crowell, *IEEE J. Quant. Elec.* 29, 944 (1993)

4. G. D. Hager, D. Kopf, D. Plummer, T. Salsich, and P. Crowell, *Chem. Phys. Lett.* 204 , 420 (1993)

5. G. D. Hager, S. A. Hanes, and M. A. Dreger, IEEE *J. Quant. Elec.* 28, 2573 (1992)

6. see, for example, S. Churassy, R. Bacis, A. J. Bouvier, C. Pierre dit Mery, B. Erba, J. Bachar, and S. Rosenwaks, *J. Appl. Phys.* 62, 31 (1987) and references therein.

7. R. F. Heidner, C. E. Gardner, G. I. Segal, and T. M. El-Sayed, *J. Phys. Chem.* 87, 2348 (1983)

8. R. F. Heidner, *J. Photochem.* 25, 449 (1984)

9. D. David, V. Joly, and A. Fausse, *"Proceedings of the 7th International Symposium on Gas Flow and Chemical Lasers"*, pp 156, Springer Proceedings in Physics, Berlin, 1987

10. G. E. Hall, W. J. Marienelli, and P. L. Houston, *J. Phys. Chem.* 87, 2153 (1983)

11. M. H. van Bentham and S. J. Davis, *J. Phys. Chem.* 90, 902 (1986)

12. P. Crozet, R. Bacis, A. Bouvier, A. J. Bouvier, S. Churassy, and J. P. Pique, *J. Phys.* C48, 385 (1987)

13. M. Nota, A. J. Bouvier, R. Bacis, A. Bouvier, P. Crozet, S. Churassy, and J. B. Koffend, *J. Chem. Phys.* 91, 1938 (1989)

14. D. Cerny, R. Bacis, A. J. Bouvier, S. Poulat, and A. Topouzkhanian, *J. Quant. Spectrosc. Radiat. Transfer*, 47, 9 (1992)

15. A. J. Bouvier, R. Bacis, A. Bouvier, D. Cerny, S. Churassy, P. Crozet, and M. Nota, *J. Quant. Spectrosc. Radiat. Transfer*, 49, 311 (1992)

16. D. L. Carroll, *AIAA 25th Plasmadynamics and Lasers Conference*, AIAA preprint 94-2431, Colorado Springs, June 1994

17. T. Ishiwata and I. Tanaka, *Laser Chem.* 7, 79 (1987)

18. S. Fei, X. Zheng, M. C. Heaven, and J. Tellinghuisen, *J. Chem. Phys.* 97, 6057 (1992)

19. S. Gerstenkorn and P. Luc, *"Atlas du Spectre d'Absorption de la Molécule d'Iode,"* Laboratoire Aime Cotton, CNRS II, Orsay, France, 1977

20. R. Bacis, D. Cerny, and F. Martin, *J. Mol. Spectrosc.* 118, 434 (1986)

21. J. Tellinghuisen, M. R. McKeever, and A. Sur, *J. Mol. Spectrosc.* 82, 225 (1980)

22. M. Bartels, R. J. Donovan, A. J. Holmes, P. R. R. Langridge-Smith, M. A. MacDonald, and T. Ridley, *J. Chem. Phys.* 91, 7355 (1989)

23. A. J. Hoy and R. H. Lipson, *Chem. Phys.* 140, 187 (1990)

24. J. Tellinghuisen, *J. Mol. Spectrosc.* 137, 248 (1989)

25. M. L. Nowlin and M. C. Heaven, *J. Chem. Phys.* 99, 5654 (1993)

26. J. Derouad and N. Sadeghi, Chem. Phys. Lett. 102, 324 (1983)

27. D. L. Carrol, private communication.

28. G. Hager, private communication.

29. X. Zheng, M. C. Heaven, and J. Tellinghuisen, *J. Mol. Spectrosc.* 164, 135 (1994)

30. J. O. Clevenger, Q. P. Ray, J. Tellinghuisen, X. Zheng, and M. C. Heaven, *Can. J. Phys.* 72, xxxx (1994)

31. J. Tellinghuisen, *Can. J. Phys.* 62, 1933 (1984)

Publications Resulting from AFOSR Support

1. X. Zheng, M. C. Heaven, and J. Tellinghuisen, *Chem. Phys. Lett.* 195, 273 (1992).
"Spectroscopy of Charge-Transfer Transitions in Jet-Cooled IBr"

2. S. Fei, X. Zheng, M. C. Heaven, and J. Tellinghuisen, *J. Chem. Phys.* 97, 6057 (1992).
"Spectroscopy and Relaxation Dynamics of I_2Ar_n Clusters: Geminate Recombination and Cluster Fragmentation"

3. M. L. Nowlin and M. C. Heaven, *J. Chem. Phys.* 99, 5654 (1993).
"Energy Transfer Rate Constants for Highly Excited Ro-vibrational Levels of $I_2(X)$".

4. M. L. Nowlin and M. C. Heaven, in *"Intense Laser Beams and Applications"*, SPIE Proceedings, Volume 1871, 290 (1993).
"Spectroscopy and Energy Transfer Dynamics of I_2 Levels in the 1-3 eV Range".

5. X. Zheng, M. C. Heaven, and J. Tellinghuisen, *J. Mol. Spectrosc.* 164, 135 (1994).
"Spectroscopy of Metastable Species in a Free-Jet Expansion: The D'-A' Transition of IBr"

6. M. L. Nowlin and M. C. Heaven, *J. Physique IV*, C4-729 (1994)
"Collisional Relaxation of Highly Excited Vibrational Levels of $I_2(X)$"

7. J. O. Clevenger, Q. P. Ray, J. Tellinghuisen, X. Zheng, and M. C. Heaven, *Can. J. Phys.* 72, xxxx (1994).
"Spectroscopy of Metastable Species in a Free-Jet Expansion: The β-A Transition of IBr"

Appendix

RKR Turning Points for $I_2(D)$

and

Franck-Condon Factors for the D-X Transition

Table A1

Rotational Constants, Vibrational Energies, and RKR Turning Points for $I_2(D)$

v	B/cm^{-1}	G(v)/cm^{-1}	R_{min}/Å	R_{max}/Å
0.	0.0206930	47.5037	3.509	3.658
1.	0.0206491	142.3323	3.458	3.717
2.	0.0206050	236.9427	3.424	3.759
3.	0.0205607	331.3305	3.397	3.794
4.	0.0205163	425.4916	3.375	3.825
5.	0.0204717	519.4220	3.355	3.853
6.	0.0204270	613.1179	3.337	3.880
7.	0.0203821	706.5756	3.321	3.904
8.	0.0203370	799.7916	3.306	3.928
9.	0.0202918	892.7626	3.292	3.950
10.	0.0202465	985.4853	3.279	3.971
11.	0.0202010	1077.9566	3.267	3.992
12.	0.0201554	1170.1737	3.255	4.012
13.	0.0201096	1262.1336	3.244	4.032
14.	0.0200638	1353.8337	3.233	4.051
15.	0.0200178	1445.2714	3.223	4.070
16.	0.0199717	1536.4443	3.214	4.088
17.	0.0199254	1627.3500	3.205	4.106
18.	0.0198791	1717.9863	3.196	4.124
19.	0.0198327	1808.3511	3.187	4.141
20.	0.0197861	1898.4423	3.179	4.158
21.	0.0197395	1988.2580	3.171	4.175
22.	0.0196927	2077.7963	3.163	4.192
23.	0.0196459	2167.0556	3.156	4.208
24.	0.0195990	2256.0341	3.149	4.225
25.	0.0195520	2344.7303	3.142	4.241
26.	0.0195049	2433.1427	3.135	4.257
27.	0.0194577	2521.2700	3.128	4.272
28.	0.0194105	2609.1107	3.121	4.288
29.	0.0193632	2696.6636	3.115	4.304
30.	0.0193159	2783.9275	3.109	4.319
31.	0.0192685	2870.9014	3.103	4.334
32.	0.0192210	2957.5841	3.097	4.350
33.	0.0191735	3043.9747	3.091	4.365
34.	0.0191259	3130.0722	3.086	4.380
35.	0.0190783	3215.8759	3.080	4.395
36.	0.0190306	3301.3848	3.075	4.409
37.	0.0189829	3386.5983	3.069	4.424
38.	0.0189352	3471.5156	3.064	4.439
39.	0.0188875	3556.1361	3.059	4.454
40.	0.0188397	3640.4593	3.054	4.468

Table A1 - continued

v	B/cm^{-1}	G(v)/cm^{-1}	R_{min}/Å	R_{max}/Å
41.	0.0187919	3724.4845	3.049	4.483
42.	0.0187441	3808.2114	3.044	4.497
43.	0.0186963	3891.6394	3.040	4.512
44.	0.0186484	3974.7682	3.035	4.526
45.	0.0186006	4057.5973	3.031	4.540
46.	0.0185528	4140.1265	3.026	4.554
47.	0.0185049	4222.3556	3.022	4.569
48.	0.0184571	4304.2842	3.017	4.583
49.	0.0184093	4385.9121	3.013	4.597
50.	0.0183615	4467.2393	3.009	4.611
51.	0.0183137	4548.2656	3.005	4.625
52.	0.0182660	4628.9909	3.001	4.639
53.	0.0182183	4709.4152	2.997	4.653
54.	0.0181706	4789.5383	2.993	4.667
55.	0.0181229	4869.3604	2.989	4.681
56.	0.0180753	4948.8815	2.985	4.695
57.	0.0180277	5028.1017	2.981	4.709
58.	0.0179802	5107.0209	2.978	4.723
59.	0.0179327	5185.6395	2.974	4.737
60.	0.0178853	5263.9575	2.970	4.751
61.	0.0178379	5341.9751	2.967	4.765
62.	0.0177906	5419.6925	2.963	4.779
63.	0.0177434	5497.1100	2.960	4.793
64.	0.0176962	5574.2279	2.956	4.806
65.	0.0176491	5651.0463	2.953	4.820
66.	0.0176021	5727.5657	2.949	4.834
67.	0.0175552	5803.7863	2.946	4.848
68.	0.0175084	5879.7085	2.943	4.862
69.	0.0174616	5955.3327	2.940	4.875
70.	0.0174150	6030.6592	2.936	4.889
71.	0.0173684	6105.6886	2.933	4.903
72.	0.0173220	6180.4212	2.930	4.917
73.	0.0172756	6254.8575	2.927	4.930
74.	0.0172294	6328.9980	2.924	4.944
75.	0.0171833	6402.8431	2.921	4.958
76.	0.0171373	6476.3934	2.918	4.972
77.	0.0170914	6549.6495	2.915	4.986
78.	0.0170456	6622.6118	2.912	4.999
79.	0.0170000	6695.2810	2.909	5.013
80.	0.0169545	6767.6577	2.906	5.027
81.	0.0169092	6839.7424	2.903	5.041
82.	0.0168639	6911.5357	2.900	5.054
83.	0.0168189	6983.0384	2.897	5.068

Table A1 - continued

v	B/cm^{-1}	G(v)/cm^{-1}	R_{min}/Å	R_{max}/Å
84.	0.0167740	7054.2511	2.895	5.082
85.	0.0167292	7125.1743	2.892	5.096
86.	0.0166846	7195.8089	2.889	5.109
87.	0.0166402	7266.1556	2.886	5.123
88.	0.0165959	7336.2149	2.884	5.137
89.	0.0165518	7405.9878	2.881	5.151
90.	0.0165078	7475.4748	2.878	5.165
91.	0.0164641	7544.6769	2.876	5.178
92.	0.0164205	7613.5947	2.873	5.192
93.	0.0163771	7682.2290	2.871	5.206
94.	0.0163339	7750.5806	2.868	5.220
95.	0.0162909	7818.6504	2.865	5.234
96.	0.0162481	7886.4392	2.863	5.247
97.	0.0162055	7953.9478	2.860	5.261
98.	0.0161631	8021.1770	2.858	5.275
99.	0.0161209	8088.1278	2.855	5.289
100.	0.0160789	8154.8009	2.853	5.303
101.	0.0160372	8221.1973	2.850	5.317
102.	0.0159956	8287.3179	2.848	5.330
103.	0.0159543	8353.1635	2.845	5.344
104.	0.0159132	8418.7352	2.843	5.358
105.	0.0158724	8484.0337	2.840	5.372
106.	0.0158318	8549.0601	2.838	5.386
107.	0.0157914	8613.8153	2.836	5.400
108.	0.0157512	8678.3003	2.833	5.414
109.	0.0157114	8742.5159	2.831	5.428
110.	0.0156717	8806.4633	2.828	5.442
111.	0.0156323	8870.1433	2.826	5.455
112.	0.0155932	8933.5570	2.824	5.469
113.	0.0155544	8996.7054	2.821	5.483
114.	0.0155158	9059.5894	2.819	5.497
115.	0.0154775	9122.2101	2.817	5.511
116.	0.0154395	9184.5685	2.814	5.525
117.	0.0154017	9246.6657	2.812	5.539
118.	0.0153642	9308.5026	2.810	5.553
119.	0.0153270	9370.0803	2.807	5.567
120.	0.0152902	9431.3999	2.805	5.581
121.	0.0152536	9492.4625	2.803	5.595
122.	0.0152173	9553.2690	2.800	5.609
123.	0.0151813	9613.8205	2.798	5.623
124.	0.0151456	9674.1182	2.796	5.637
125.	0.0151102	9734.1631	2.794	5.651

Table A2

Franck-Condon Factors for the D-X System of I_2

v"	v' = 4	v' = 5	v' = 6	v' = 7
21	8.0573E-14	6.2078E-13	4.0116E-12	2.2360E-11
22	5.5414E-13	4.1028E-12	2.5471E-11	1.3634E-10
23	3.5730E-12	2.5380E-11	1.5111E-10	7.7540E-10
24	2.1620E-11	1.4707E-10	8.3819E-10	4.1152E-09
25	1.2285E-10	7.9879E-10	4.3490E-09	2.0385E-08
26	6.5592E-10	4.0677E-09	2.1109E-08	9.4246E-08
27	3.2912E-09	1.9422E-08	9.5835E-08	4.0649E-07
28	1.5521E-08	8.6932E-08	4.0676E-07	1.6343E-06
29	6.8774E-08	3.6459E-07	1.6128E-06	6.1185E-06
30	2.8624E-07	1.4317E-06	5.9674E-06	2.1297E-05
31	1.1182E-06	5.2586E-06	2.0572E-05	6.8781E-05
32	4.0958E-06	1.8038E-05	6.5950E-05	2.0557E-04
33	1.4048E-05	5.7681E-05	1.9610E-04	5.6667E-04
34	4.5045E-05	1.7154E-04	5.3915E-04	1.4347E-03
35	1.3473E-04	4.7302E-04	1.3650E-03	3.3179E-03
36	3.7486E-04	1.2049E-03	3.1659E-03	6.9592E-03
37	9.6703E-04	2.8217E-03	6.6822E-03	1.3115E-02
38	2.3031E-03	6.0383E-03	1.2723E-02	2.1923E-02
39	5.0369E-03	1.1714E-02	2.1590E-02	3.1903E-02
40	1.0045E-02	2.0379E-02	3.2106E-02	3.9282E-02
41	1.8100E-02	3.1326E-02	4.0777E-02	3.8988E-02
42	2.9103E-02	4.1618E-02	4.2394E-02	2.8314E-02
43	4.1009E-02	4.6133E-02	3.3264E-02	1.1591E-02
44	4.9270E-02	4.0035E-02	1.6119E-02	4.7852E-04
45	4.8172E-02	2.3607E-02	1.8991E-03	5.0983E-03
46	3.4945E-02	5.8136E-03	2.7669E-03	2.1071E-02
47	1.4715E-02	4.3360E-04	1.8517E-02	2.9271E-02

v"	v' = 8	v' = 9	v' = 10	v' = 11
21	1.0972E-10	4.8145E-10	1.9122E-09	6.9424E-09
22	6.4228E-10	2.7043E-09	1.0302E-08	3.5859E-08
23	3.5001E-09	1.4114E-08	5.1468E-08	1.7137E-07
24	1.7763E-08	6.8455E-08	2.3840E-07	7.5760E-07
25	8.3952E-08	3.0847E-07	1.0234E-06	3.0955E-06
26	3.6940E-07	1.2907E-06	4.0679E-06	1.1676E-05
27	1.5122E-06	5.0091E-06	1.4950E-05	4.0580E-05
28	5.7524E-06	1.8006E-05	5.0704E-05	1.2963E-04
29	2.0305E-05	5.9826E-05	1.5829E-04	3.7942E-04
30	6.6370E-05	1.8326E-04	4.5332E-04	1.0132E-03
31	2.0036E-04	5.1578E-04	1.1859E-03	2.4547E-03
32	5.5670E-04	1.3279E-03	2.8177E-03	5.3568E-03
33	1.4175E-03	3.1095E-03	6.0357E-03	1.0427E-02

Table A2 - Continued

v"	v' = 8	v' = 9	v' = 10	v' = 11
34	3.2891E-03	6.5740E-03	1.1541E-02	1.7860E-02
35	6.9040E-03	1.2423E-02	1.9427E-02	2.6396E-02
36	1.2981E-02	2.0697E-02	2.8217E-02	3.2647E-02
37	2.1570E-02	2.9790E-02	3.4267E-02	3.2053E-02
38	3.1059E-02	3.5901E-02	3.2945E-02	2.2419E-02
39	3.7589E-02	3.4295E-02	2.2381E-02	8.2013E-03
40	3.6273E-02	2.3171E-02	7.6913E-03	8.0793E-05
41	2.5049E-02	7.9139E-03	1.5700E-05	5.7884E-03
42	9.0798E-03	1.3433E-05	6.7283E-03	1.8901E-02
43	8.4013E-05	7.0523E-03	2.0366E-02	2.2252E-02
44	6.5588E-03	2.1386E-02	2.3156E-02	9.9762E-03
45	2.1771E-02	2.4604E-02	9.9611E-03	2.1600E-05
46	2.6701E-02	1.0946E-02	2.8030E-06	8.9155E-03
47	1.3301E-02	2.4549E-05	9.8185E-03	2.0836E-02

v"	v' = 12	v' = 13	v' = 14	v' = 15
21	2.3228E-08	7.2103E-08	2.0884E-07	5.6718E-07
22	1.1496E-07	3.4173E-07	9.4728E-07	2.4604E-06
23	5.2525E-07	1.4917E-06	3.9472E-06	9.7784E-06
24	2.2142E-06	5.9913E-06	1.5091E-05	3.5547E-05
25	8.6030E-06	2.2111E-05	5.2837E-05	1.1792E-04
26	3.0755E-05	7.4819E-05	1.6897E-04	3.5579E-04
27	1.0093E-04	2.3146E-04	4.9179E-04	9.7208E-04
28	3.0313E-04	6.5208E-04	1.2964E-03	2.3908E-03
29	8.2978E-04	1.6646E-03	3.0761E-03	5.2517E-03
30	2.0593E-03	3.8249E-03	6.5142E-03	1.0193E-02
31	4.6009E-03	7.8395E-03	1.2169E-02	1.7215E-02
32	9.1672E-03	1.4156E-02	1.9725E-02	2.4731E-02
33	1.6078E-02	2.2122E-02	2.7056E-02	2.9140E-02
34	2.4357E-02	2.9120E-02	3.0145E-02	2.6360E-02
35	3.0961E-02	3.0851E-02	2.5259E-02	1.5791E-02
36	3.1423E-02	2.4079E-02	1.3238E-02	3.7357E-03
37	2.3058E-02	1.1046E-02	1.9954E-03	4.0020E-04
38	9.3408E-03	9.0181E-04	1.4736E-03	9.1106E-03
39	3.2084E-04	2.9184E-03	1.2086E-02	1.8935E-02
40	4.4429E-03	1.4759E-02	2.0296E-02	1.5687E-02
41	1.7035E-02	2.1113E-02	1.3855E-02	3.2898E-03
42	2.1665E-02	1.2117E-02	1.5988E-03	1.5255E-03
43	1.0756E-02	6.1266E-04	3.3890E-03	1.3383E-02
44	1.6042E-04	5.4562E-03	1.5964E-02	1.6026E-02
45	7.3862E-03	1.7952E-02	1.4900E-02	3.5048E-03
46	1.9500E-02	1.3661E-02	1.7259E-03	2.3336E-03
47	1.2706E-02	6.8912E-04	4.6028E-03	1.5090E-02

Table A2 - Continued

v''	v' = 16	v' = 17	v' = 18	v' = 19
21	1.4503E-06	3.5047E-06	8.0287E-06	1.7485E-05
22	6.0125E-06	1.3873E-05	3.0320E-05	6.2930E-05
23	2.2770E-05	5.0013E-05	1.0393E-04	2.0484E-04
24	7.8614E-05	1.6378E-04	3.2233E-04	6.0072E-04
25	2.4671E-04	4.8542E-04	9.0057E-04	1.5787E-03
26	7.0095E-04	1.2958E-03	2.2531E-03	3.6907E-03
27	1.7932E-03	3.0949E-03	5.0063E-03	7.5986E-03
28	4.1006E-03	6.5534E-03	9.7686E-03	1.3581E-02
29	8.2993E-03	1.2150E-02	1.6470E-02	2.0632E-02
30	1.4661E-02	1.9365E-02	2.3415E-02	2.5762E-02
31	2.2150E-02	2.5802E-02	2.6972E-02	2.4907E-02
32	2.7713E-02	2.7405E-02	2.3364E-02	1.6411E-02
33	2.7147E-02	2.1133E-02	1.2775E-02	4.9293E-03
34	1.8509E-02	9.2554E-03	2.1827E-03	4.2879E-05
35	6.1765E-03	5.3990E-04	1.0802E-03	6.6294E-03
36	5.3369E-07	3.2261E-03	1.0402E-02	1.6170E-02
37	6.0449E-03	1.3933E-02	1.7806E-02	1.4742E-02
38	1.6831E-02	1.8080E-02	1.1956E-02	3.6992E-03
39	1.7239E-02	8.7488E-03	1.1949E-03	9.1570E-04
40	5.7268E-03	6.7484E-05	3.3838E-03	1.1113E-02
41	2.7868E-04	6.7148E-03	1.4254E-02	1.4201E-02
42	1.0217E-02	1.6083E-02	1.2053E-02	3.3334E-03
43	1.6573E-02	9.0729E-03	8.8020E-04	1.8643E-03
44	6.0382E-03	2.0878E-06	5.1061E-03	1.2910E-02
45	6.2412E-04	8.8789E-03	1.4663E-02	9.4754E-03
46	1.2362E-02	1.4631E-02	5.9151E-03	2.8129E-06
47	1.3234E-02	2.7761E-03	9.6820E-04	9.2594E-03